JOURNAL OF GUIDANCE, CONTROL, AND DYNAMICS
Vol. 38, No. 1, January 2015

Adaptive Attitude-Tracking Control of Spacecraft with Uncertain Time-Varying Inertia Parameters

Divya Thakur*
University of Texas at Austin, Austin, Texas 78712-1221
Sukumar Srikant†
Indian Institute of Technology, Bombay, Mumbai 400 076, India
and
Maruthi R. Akella‡
University of Texas at Austin, Austin, Texas 78712-1221

DOI: 10.2514/1.G000457

Although adaptive control schemes for spacecraft attitude tracking are abundant in controls literature, very few are designed to guarantee consistent performance for a spacecraft with both rigid and nonrigid (time-varying) inertia components. Because inertia matrix changes are a common occurrence due to phenomena like fuel depletion or mass displacement in a deployable spacecraft, an adaptive control algorithm that takes explicit account of such information is of significant interest. In this paper, a novel adaptive attitude control scheme is presented for a spacecraft with inertia matrix parameters that have both unknown rigid components and only partially determined variable components. The proposed controller directly compensates for inertia variations that occur as either pure functions of the control input, or as functions of time. For the particular case of an input-dependent inertia matrix, a bounded control solution is ensured by placing some mild restrictions on the initial conditions and by employing a smooth projection scheme that confines the parameter estimates to a well-dMefined convex set. Detailed derivations of the control law are provided, along with a thorough analysis for the associated stability and error convergence properties. In addition, numerical simulations are presented to highlight the performance benefits when compared with an adaptive control scheme that does not account for inertia variations.

I. Introduction

THE attitude control problem of a rigid body is a widely researched field with several elegant solutions addressing application-specific constraints. Among these solutions, a significant amount of work is geared toward addressing the problem of unknown or uncertain system parameters using adaptive control techniques [1–6]. In the context of spacecraft attitude tracking, adaptive control theory has been applied extensively to account for mass properties that cannot be exactly determined during prefight testing. The majority of available adaptive attitude-tracking control literature is, however, focused on rigid spacecraft with uncertain parameters that are constant and do not display any time variation. Although this assumption may be suitable for some spacecraft with very slowly varying system parameters, a growing number of missions anticipate having to incorporate spacecraft with rapidly deployable appendages coupled with fast propulsive maneuvers, which result in appreciable variations in the inertia parameters. For example, in a deployable spacecraft, an expanding solar array or sensor boom causes mass displacement. Similarly, a spacecraft undergoing demanding rotational or translational maneuvers rapidly loses a significant amount of mass due to fuel depletion. In both cases, the result is a system with a time-varying inertia profile that must be taken into consideration for precise attitude-tracking requirements.

Classical literature in the area of adaptive control has addressed the problem of time-varying plant parameters but for linear dynamic systems. The methodology in [7] considers linear systems with time-varying parameters in a compact set, whereas [8,9] address linear systems with unknown but slowly time-varying parametric uncertainties. A thorough presentation of many technically rich results in robust adaptive control can be found in [10]. More recent results provide extensions to limited classes of nonlinear time-varying plants. The formulation of [11] accounts for nonlinear plants with unknown periodic time-varying uncertainties that may be rapidly time varying but have known periodicity. Ge and Wang [12] examine a single-input/single-output nonlinear system with unknown control coefficients and uncertain time-varying parameters belonging to known compact sets. The robust adaptive tracking control law proposed in [12] ensures global uniform ultimate boundedness of the closed-loop system signal, whereas asymptotic stability is only guaranteed if the unknown parameters are constant. A recent result in [13] addresses the problem of achieving fast parameter adaptation through high-gain learning rates by employing a novel robustness modification technique to filter out high-frequency oscillations incurred in the control response as a result of the high-gain learning rates. The result is applied to the rigid-body stabilization problem in [14] where flexible modes are treated as perturbations in the system dynamics. Although the result in [13,14] is a novel contribution in the area of robust adaptive control, it does not explicitly account for system dynamics resulting from time-varying parameters that exhibit rapid and persistent changes over time.

This paper treats the problem of adaptive control for the highly nonlinear rigid body dynamics to account for time-varying system (inertia matrix) parameters with multiplicative and additive uncertainties. The problem formulation and corresponding solution approach presented in this paper are both motivated by the underlying assumption that inertia matrix variations often occur as a result of a known dynamic phenomena. Although this assumption may appear restrictive, in fact, it readily serves many practical applications. For example, in the case of mass loss due to fuel consumption, the rate of change of the spacecraft mass is known to be a function of the applied control and actuator hardware characteristics. Inertia parameter variations arising due to mass displacement caused by deploying

Received 20 December 2013; revision received 10 May 2014; accepted for publication 7 September 2014; published online 1 December 2014.

*Ph.D. Candidate, Department of Aerospace Engineering and Engineering Mechanics, 1 University Station, Code C0600.
†Assistant Professor, Systems and Control Engineering, Powai.
‡Associate Professor, Department of Aerospace Engineering and Engineering Mechanics, 1 University Station, Code C0600. Associate Fellow AIAA.

appendages, as well as any other time- or state-dependent inertia parameters could also be treated within this framework. In particular, the variable component of the inertia matrix is assumed to evolve according to known dynamics that may be periodic or nonperiodic, vanishing or persistent, and may depend on either time or the control input. Although the variation is well characterized, the overall bounds on the inertia matrix are assumed to be unknown. This assumption is relaxed for the particular case of input-dependent inertia parameters wherein prior knowledge is used to construct a smooth parameter projection scheme to bound the parameter estimates within a convex region. The smooth projections mechanism is crucial for ensuring a bounded control solution for the coupled dynamics resulting from a control-dependent inertia matrix. The proposed adaptive control law ensures (almost) global asymptotic stability of the closed-loop tracking errors. Unlike [13,14], the work presented in this paper explicitly accounts for time variations arising in the unknown parameters rather than relying on high-gain learning rates and robustness modification techniques. As a result, the proposed adaptive control result is specifically formulated and customized for the particular type of inertia-matrix variation stemming from the application under consideration.

Weiss et al. [15] address a similar problem wherein the inertia matrix description is provided as an unknown constant component, as well as a time-varying component of known variation profile but unknown bound. Similar to [15], the adaptive control method dealing with time-dependent inertia parameters presented in this paper does not require knowledge of a lower or upper bound on the inertia matrix. However, the formulation in [15] only considers variations in the inertia matrix of a purely time-dependent nature. The salient and distinguishing feature of our novel control method is its ability to handle not only time-dependent, but also a combination of time- and state-dependent or, by assuming some knowledge on the overall bounds of the inertia matrix, purely input-dependent variations in the inertia matrix.

The adaptive attitude-tracking control strategy proposed in this study is based on the classical certainty-equivalence (CE) principle [16]. The attitude measurements, given in terms of the singularity-free unit quaternion, and the corresponding body angular rates are assumed to be perfectly measured and available for feedback. It is important to note here that, when quaternion-based formulations are used to parameterize the set of rotation matrices $SO(3)$ it is impossible to obtain a globally stabilizing controller using continuous feedback [1]. Based on these well-known limitations, the authors adopt the standard terminology of (almost) global stability, which implies stability over $S(3)$ or $\mathbb{R}^3$ [1,3]. Thus, assuming an uncertain time-varying inertia matrix, the proposed control method delivers (almost) globally stabilizing closed-loop performance with asymptotic tracking of any reference trajectory for most initial conditions. When dealing with an input-dependent inertia matrix, some reasonably mild restrictions on the initial conditions are necessary to guarantee a bounded control input. In addition, a smooth projection scheme is implemented to bound the parameter estimates within a well-defined convex set, to avoid any singularity issues in the proposed controller.

In the development that follows, the attitude and angular velocity tracking error dynamics for a spacecraft with time-varying inertia matrix are derived in Sec. II. The main results of the paper along with stability analysis are presented in Secs. III and IV: In Sec. III, the control method is presented for time- and state-dependent inertia matrices, whereas in Sec. IV, the control method is extended to handle an input-dependent inertia matrix. In Sec. V, numerical simulations are provided for spacecraft appendage deployment and fuel-loss scenarios. Finally, in Sec. VI, concluding remarks summarize presented results.

II. Problem Statement

A. Kinematics and Dynamics of a Nonrigid Spacecraft

A complete kinematic and dynamic description for a nonrigid body is provided using Euler parameters (quaternions) and Euler's rotational equations of motion. The Euler parameter kinematic differential equations are written as [17]

$$\dot{\boldsymbol{q}}(t) = \frac{1}{2}E(\boldsymbol{q}(t))\boldsymbol{\omega}(t); \qquad E(\boldsymbol{q}(t)) = \begin{bmatrix} -\boldsymbol{q}_v^T \\ q_0\boldsymbol{I} + S(\boldsymbol{q}_v) \end{bmatrix} \tag{1}$$

where $\boldsymbol{q}(t) \in \mathbb{R}^4$ is the unit norm constrained quaternion vector composed of scalar and vector components denoted respectively as $q_0 \in \mathbb{R}$ and $\boldsymbol{q}_v \in \mathbb{R}^3$ (i.e., $\boldsymbol{q} = [q_0, \boldsymbol{q}_v^T]^T$ and $\boldsymbol{q}^T\boldsymbol{q} = 1$), and $S(\cdot)$ is the matrix representation of the linear cross-product operation such that $S(\boldsymbol{a})\boldsymbol{b} = \boldsymbol{a} \times \boldsymbol{b}$ for any $\boldsymbol{a}, \boldsymbol{b} \in \mathbb{R}^3$. In Eq. (1), $\boldsymbol{\omega}(t) \in \mathbb{R}^3$ is the angular velocity of the body as expressed in a rotating body-fixed reference frame, whereas $\boldsymbol{I}$ is the 3×3 identity matrix. The attitude dynamics of the nonrigid body are governed by the following rotational equations of motion:

$$J(t)\dot{\boldsymbol{\omega}}(t) = -\dot{J}(t)\boldsymbol{\omega}(t) - S(\boldsymbol{\omega}(t))J(t)\boldsymbol{\omega}(t) + \boldsymbol{u}(t) \tag{2}$$

where $J(t)$ is the 3×3 time-varying, symmetric positive-definite mass moment of inertia matrix of the spacecraft and $\boldsymbol{u}(t) \in \mathbb{R}^3$ is the external control torque. Note that, for notational convenience, the time argument t is hereafter left out, unless specifically stated for clarification or emphasis. The direction cosine matrix $C(\boldsymbol{q})$ denotes a transformation from inertial reference frame $\mathcal{N}$ to body-fixed reference $\mathcal{B}$ (i.e., $\mathcal{N} \to \mathcal{B}$) and can be parameterized in terms of $\boldsymbol{q}$ as follows [17,18]:

$$C(\boldsymbol{q}) = (q_0^2 - \boldsymbol{q}_v^T\boldsymbol{q}_v)I + 2\boldsymbol{q}_v\boldsymbol{q}_v - 2q_0S(\boldsymbol{q}_v)$$

Because the reference angular velocity is often prescribed in its own reference frame $\mathcal{R}$, the rotation given by $\mathcal{R} \to \mathcal{B}$ is obtained by combining the corresponding rotation matrices $C(\boldsymbol{q})$ and $C(\boldsymbol{q}_r)$ into a single rotation matrix $C(\boldsymbol{q}_e)$ as follows:

$$C(\boldsymbol{q}_e) = C(\boldsymbol{q})(C(\boldsymbol{q}_r))^T \tag{3}$$

where $\boldsymbol{q}_e = [q_{e0}, \boldsymbol{q}_{e_v}^T]^T$ denotes the error between the spacecraft $\boldsymbol{q}$ and reference $\boldsymbol{q}_r$ quaternion states. The angular velocity tracking error is expressed as

$$\boldsymbol{\omega}_e = \boldsymbol{\omega} - C(\boldsymbol{q}_e)\boldsymbol{\omega}_r \tag{4}$$

where $\boldsymbol{\omega}_r$ is the bounded reference angular velocity. The complete attitude-tracking error dynamics are obtained by differentiating Eqs. (3) and (4) with respect to time [1–3,17], thus yielding

$$\dot{\boldsymbol{q}}_e = \frac{1}{2}E(\boldsymbol{q}_e)\boldsymbol{\omega}_e \tag{5}$$

$$\dot{\boldsymbol{\omega}}_e = J^{-1}(-\dot{J}\boldsymbol{\omega} - S(\boldsymbol{\omega})J\boldsymbol{\omega} + \boldsymbol{u}) + S(\boldsymbol{\omega}_e)C(\boldsymbol{q}_e)\boldsymbol{\omega}_r - C(\boldsymbol{q}_e)\dot{\boldsymbol{\omega}}_r \tag{6}$$

B. Characterization of Time-Varying Inertia Matrix

The particular time-varying inertia matrix model treated in the upcoming adaptive control law development is expressed according to

$$J(t) = J_0 - J_1\Psi(t) \tag{7}$$

where $J_0 \in \mathbb{R}^{3\times3}$, $J_0 = J_0^T > 0$ is an unknown, constant matrix that represents the rigid portion of the spacecraft, and $J_1\Psi$ is the nonrigid component of the spacecraft that satisfies

$$J_1\Psi \in \mathbb{R}^{3\times3}, \qquad J_1\Psi = \Psi^T J_1^T \tag{8}$$

In particular, $J_1 \in \mathbb{R}^{3\times n}$ is unknown and constant, whereas $\Psi(t) \in \mathbb{R}^{n\times3}$ is known and time dependent for any $n > 0$. In Eq. (7), observe that J is the difference of two symmetric matrices, which ensures $J = J^T$ for all $t \geq 0$. Moreover, although $J_1\Psi$ itself may be sign indefinite, it must ensure that $J = J_0 - J_1\Psi > 0$ for all time. In addition, to guarantee a physically possible distribution of mass,

careful consideration should be given during the mathematical modeling process to ensure that the inertia matrix satisfies the following triangle inequalities for all time [19]:

$$\tilde{J}_1 + \tilde{J}_2 \geq \tilde{J}_3, \qquad \tilde{J}_2 + \tilde{J}_3 \geq \tilde{J}_1, \qquad \tilde{J}_3 + \tilde{J}_1 \geq \tilde{J}_2 \tag{9}$$

where $\tilde{J}_1$, $\tilde{J}_2$, and $\tilde{J}_3$ are the principal moments of inertia of the spacecraft.

We now examine specific details regarding the structure of J_1 and Ψ. In particular, mathematical characterizations are provided for a time- and/or state-dependent inertia matrix for mass displacement due to phenomena such as deploying appendages, as well as an input $\boldsymbol{u}$ dependent inertia matrix that models mass loss due to fuel expenditure. Pertinent details related to the structure of $J_1\Psi$ are provided along with illustrative examples.

1. *Time- and/or State-Dependent Inertia Matrix*

When variations in J have explicit dependence on time or the spacecraft state $\boldsymbol{x} = [\boldsymbol{q}_{e_v}^T, \boldsymbol{\omega}^T]^T$, the time derivative of Eq. (7) is given by

$$\dot{J}(t) = -J_1\dot{\Psi}(t, \boldsymbol{x}(t)) \tag{10}$$

where $\dot{\Psi}(t, \boldsymbol{x}(t))$ is known and well characterized. If the inertia matrix in Eq. (10) is purely dependent on time, as is the case for a deploying appendage, the argument $\boldsymbol{x}$ would be dropped so that $\dot{\Psi} = \Psi(t)$.

To illustrate the efficacy of Eqs. (7) and (10) for moving mass problems, consider the example of a spacecraft shown in Fig. 1 with deploying parts. Let $\tilde{J}_0$ represent the spacecraft's main body's inertia matrix relative to O, the spacecraft's center of mass, determined in the body-fixed frame $\mathcal{B}$ with basis $\boldsymbol{b} = \{\hat{\boldsymbol{b}}_1, \hat{\boldsymbol{b}}_2, \hat{\boldsymbol{b}}_3\}$. The center of mass of a moving object with unknown constant mass m_1 is located at a position $\boldsymbol{\rho}_1(t) = \rho_{1_1}(t)\hat{\boldsymbol{b}}_1 + \rho_{1_2}(t)\hat{\boldsymbol{b}}_2 + \rho_{1_3}(t)\hat{\boldsymbol{b}}_3$ relative to O. This object has an unknown moment of inertia J'_{m_1} relative to a set of parallel axes located at $\boldsymbol{\rho}_1$. Another moving object with unknown mass m_2 is located at a different position $\boldsymbol{\rho}_2(t)$ (relative to O) and is characterized by an unknown inertia matrix J'_{m_2} relative to a parallel set of axes at its own center of mass. Observe that both position vectors $\boldsymbol{\rho}_1(t)$ and $\boldsymbol{\rho}_2(t)$ are known functions of time that are each bounded and smooth.

Through an application of the parallel-axis theorem, and assuming that the spacecraft center of mass is unaffected by mass movement, the overall inertia matrix of the spacecraft is given by

$$J = \tilde{J}_0 + J'_{m_1} + m_1[\boldsymbol{\rho}_1^T\boldsymbol{\rho}_1\boldsymbol{I} - \boldsymbol{\rho}_1\boldsymbol{\rho}_1^T] + J'_{m_2} + m_2[\boldsymbol{\rho}_2^T\boldsymbol{\rho}_2\boldsymbol{I} - \boldsymbol{\rho}_2\boldsymbol{\rho}_2^T] \tag{11}$$

which is easily written in the form of Eq. (7) with J_0 given by

$$J_0 = \tilde{J}_0 + J'_{m_1} + J'_{m_2} \tag{12}$$

and $J_1\Psi$ expressed as

$$J_1\Psi = -[m_1\boldsymbol{I} \quad m_2\boldsymbol{I}]\begin{bmatrix}\boldsymbol{\rho}_1^T(t)\boldsymbol{\rho}_1(t)\boldsymbol{I} - \boldsymbol{\rho}_1(t)\boldsymbol{\rho}_1^T(t) \\ \boldsymbol{\rho}_2^T(t)\boldsymbol{\rho}_2(t)\boldsymbol{I} - \boldsymbol{\rho}_2(t)\boldsymbol{\rho}_2^T(t)\end{bmatrix} \tag{13}$$

where $\boldsymbol{I}$ is the 3×3 identity matrix, $J_1 \in \mathbb{R}^{3\times 6}$ is unknown and constant, and $\Psi \in \mathbb{R}^{6\times 3}$ is known and time dependent and can be easily differentiated to obtain $\dot{\Psi}(t)$.

2. *Input-Dependent Inertia Matrix*

For the specific case of spacecraft undergoing fuel loss, the matrix $\dot{\Psi}$ depends explicitly on the control vector components $\boldsymbol{u}$, such that

$$\dot{J}(t) = -J_1\dot{\Psi}(\boldsymbol{u}(t)) \tag{14}$$

Observe that

$$\Psi = \int_0^t \dot{\Psi}(\boldsymbol{u}(\tau))\,\mathrm{d}\tau$$

can be numerically computed for feedback. It is important to note that no general mass depletion model exists in this regard, and that the structure of $\dot{\Psi}$ is a factor of the propulsion system, and more specifically, the propellant reservoir/tank configuration within the spacecraft.

One particular model for fuel loss is discussed next, wherein a single propellant tank is assumed to undergo uniform mass loss as a result of control torque action. The center of mass P of the tank is located at at $\boldsymbol{\rho} = \rho_1\hat{\boldsymbol{b}}_1 + \rho_2\hat{\boldsymbol{b}}_2 + \rho_3\hat{\boldsymbol{b}}_3$ relative to the known spacecraft mass center O. It is reasonable to assume that the fuel tank's principal axes are parallel with the body-fixed axes. The configuration, as illustrated in Fig. 2, is applicable to many existing spacecraft, especially for spacecraft of smaller scale such as microsatellites.

The inertia matrix of the spacecraft's main body, relative to its center of mass O, is denoted by J_0. The principal moment of inertia matrix of the fuel tank relative to P is denoted as $J_f(t)$ and derived as follows. Using the mass relation

$$\dot{m}_f(t) = -c\|\boldsymbol{u}\|; \qquad m_f(0) = m_{f_0} \tag{15}$$

where $m_f(t)$ is the time-varying mass of the propellant tank, $m_{f_0} > 0$ is its fuel mass at time $t = 0$, and the constant $c > 0$, which relates the

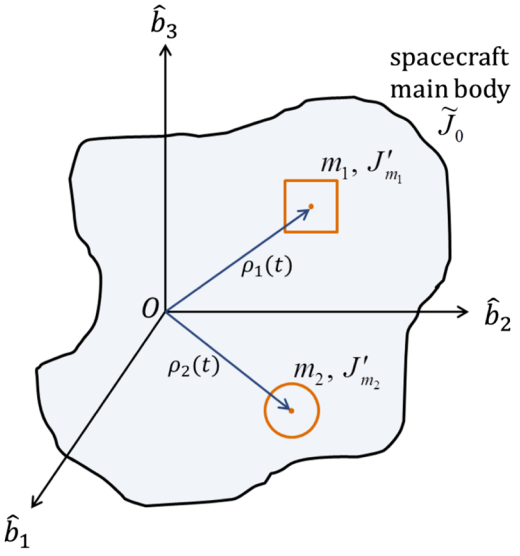

Fig. 1 Spacecraft with mass displacement due to deploying appendages.

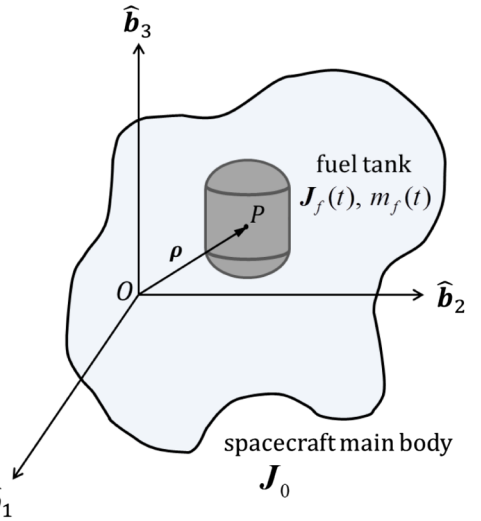

Fig. 2 Spacecraft with a single propellant tank undergoing fuel mass loss proportionate to the commanded control torque.

control torque $\boldsymbol{u}$ to mass loss, is imprecisely determined, and ignoring slosh effects, it can be shown that J_f evolves according to the dynamic equation

$$\dot{J}_f = -\text{diag}\{\alpha_1, \alpha_2, \alpha_3\}\|\boldsymbol{u}\| \tag{16}$$

where $\alpha_i = d_i c > 0$ for all $i = 1, 2, 3$ is an unknown constant given as the product of the torque-to-mass relational constant c and the constant $d_i > 0$, which depends on the dimension and shape of the fuel tank. For example, if the fuel tank is a sphere of radius r, then $d_i = (2/5)r^2$. The expression in Eq. (16) can be readily integrated to obtain J_f relative to P. Next, applying the parallel-axis theorem to determine J_f relative to O leads to the expression $-J_1\Psi = J_f + m_f(t)[\boldsymbol{\rho}^T\boldsymbol{\rho}\boldsymbol{I} - \boldsymbol{\rho}\boldsymbol{\rho}^T]$, where $J_1\Psi$ represents the variable component of the overall spacecraft inertia matrix J. Differentiating this expression and using the mass change relation in Eq. (15) together with Eq. (16) yields the following dynamic equation governing the evolution of the matrix $J_1\Psi$:

$$-J_1\dot{\Psi}(\boldsymbol{u}) = -\underbrace{(\text{diag}\{\alpha_1, \alpha_2, \alpha_3\} + c[\boldsymbol{\rho}^T\boldsymbol{\rho}\boldsymbol{I} - \boldsymbol{\rho}\boldsymbol{\rho}^T])}_{J_1}\underbrace{\|\boldsymbol{u}\|I}_{\dot{\Psi}(u)} \tag{17}$$

where J_1 is symmetric, positive definite, and unknown, and $\dot{\Psi}(\boldsymbol{u}) = \|\boldsymbol{u}\|I$.

Finally, with the dynamic model and inertia matrix characterizations in place, the control objective is now stated. The adaptive control objective is to track any prescribed reference trajectory $[\boldsymbol{q}_r(t), \boldsymbol{\omega}_r(t)]$, with bounded and smooth $\boldsymbol{\omega}_r(t)$, for all initial conditions $[\boldsymbol{q}(0), \boldsymbol{\omega}(0)]$, assuming full-state feedback and arbitrarily large uncertainty in the J_0 and J_1 matrix components. That is, a control torque $\boldsymbol{u}$ needs to be designed such that the tracking error signals converge $\lim_{t\to\infty}[\boldsymbol{q}_{e_v}(t), \boldsymbol{\omega}_e(t)] = 0$, while ensuring that all closed-loop signals remain bounded at all times. Subsequent control development will specifically treat inertia matrices described according to Eqs. (10) and (17).

III. Adaptive Attitude Tracking for Unknown Inertia with Time and State Dependencies

In this section, a novel adaptive control law is presented for the attitude and angular velocity tracking problem described by Eqs. (5) and (6) for an unknown time-varying inertia matrix composed of only state- and time-dependent terms and that evolves according to Eq. (10). First, to facilitate the adaptive controller development, some pertinent definitions and algebraic manipulations are introduced. To begin with, the dynamics of Eq. (6) are rearranged into a parameter-affine form through the judicious addition and subtraction of the terms

$$-\frac{1}{2}[q_{e0}\boldsymbol{I} + S(\boldsymbol{q}_{e_v})]\boldsymbol{\omega}_e - J^{-1}\beta\boldsymbol{q}_{e_v} - J^{-1}k_v\boldsymbol{\omega}_e - \frac{1}{2}J^{-1}\dot{J}[\boldsymbol{\omega}_e + \boldsymbol{q}_{e_v}]$$

where β, $k_v > 0$. Thus,

$$\begin{aligned}\dot{\boldsymbol{\omega}}_e = &-\frac{1}{2}[q_{e0}\boldsymbol{I} + S(\boldsymbol{q}_{e_v})]\boldsymbol{\omega}_e - J^{-1}\beta\boldsymbol{q}_{e_v} - J^{-1}k_v\boldsymbol{\omega}_e - \frac{1}{2}J^{-1}\dot{J}[\boldsymbol{\omega}_e + \boldsymbol{q}_{e_v}]\\ &+ J^{-1}\left(\boldsymbol{u} + \frac{1}{2}J[q_{e_0}\boldsymbol{I} + S(\boldsymbol{q}_{e_v})]\boldsymbol{\omega}_e + \beta\boldsymbol{q}_{e_v} + k_v\boldsymbol{\omega}_e\right.\\ &\left. + \frac{1}{2}\dot{J}[\boldsymbol{\omega}_e + \boldsymbol{q}_{e_v}] - S(\boldsymbol{\omega})J\boldsymbol{\omega} - \dot{J}\boldsymbol{\omega} + J\boldsymbol{\phi}\right)\end{aligned} \tag{18}$$

where $\boldsymbol{\phi} = S(\boldsymbol{\omega}_e)C(\boldsymbol{q}_e)\boldsymbol{\omega}_r - C(\boldsymbol{q}_e)\dot{\boldsymbol{\omega}}_r$. Recalling that $J = J_0 - J_1\Psi$ and $\dot{J} = -J_1\dot{\Psi}$ and following through with some minor algebraic manipulations, it is straightforward to obtain

$$\begin{aligned}\dot{\boldsymbol{\omega}}_e = &-\frac{1}{2}[q_{e0}I + S(\boldsymbol{q}_{e_v})]\boldsymbol{\omega}_e - J^{-1}\beta\boldsymbol{q}_{e_v} - J^{-1}k_v\boldsymbol{\omega}_e + \frac{1}{2}J^{-1}J_1\dot{\Psi}[\boldsymbol{\omega}_e + \boldsymbol{q}_{e_v}]\\ &+ J^{-1}\left(\boldsymbol{u} + \beta\boldsymbol{q}_{e_v} + k_v\boldsymbol{\omega}_e + J_0\left(\frac{1}{2}[q_{e_0}I + S(\boldsymbol{q}_{e_v})]\boldsymbol{\omega}_e + \boldsymbol{\phi}\right)\right.\\ &- S(\boldsymbol{\omega})J_0\boldsymbol{\omega} - J_1\Psi\left(\frac{1}{2}[q_{e_0}I + S(\boldsymbol{q}_{e_v})]\boldsymbol{\omega}_e + \boldsymbol{\phi}\right)\\ &\left. + S(\boldsymbol{\omega})J_1\Psi\boldsymbol{\omega} + J_1\dot{\Psi}\left\{\omega - \frac{1}{2}[\boldsymbol{\omega}_e + \boldsymbol{q}_{e_v}]\right\}\right)\end{aligned} \tag{19}$$

In Eq. (19), notice that J_0 multiplies terms in a linear fashion, thus allowing the regressor matrix W_1 to be constructed in the following manner

$$W_1\boldsymbol{\theta}^* = J_0\left(\frac{1}{2}[q_{e_0}I + S(\boldsymbol{q}_{e_v})]\boldsymbol{\omega}_e + \boldsymbol{\phi}\right) - S(\boldsymbol{\omega})J_0\boldsymbol{\omega} \tag{20}$$

where $\boldsymbol{\theta}^* = [J_{0_{11}}, J_{0_{12}}, J_{0_{13}}, J_{0_{22}}, J_{0_{23}}, J_{0_{33}}]^T$ contains the six unique parameters of J_0. Similarly, J_1 also multiplies terms linearly in Eq. (19), which allows the regressor matrix definitions for W_2 and W_3 to be given by

$$W_2\boldsymbol{\sigma}^* = -J_1\Psi\left(\frac{1}{2}[q_{e_0}I + S(\boldsymbol{q}_{e_v})]\boldsymbol{\omega}_e + \boldsymbol{\phi}\right) + S(\boldsymbol{\omega})J_1\Psi\boldsymbol{\omega} \tag{21}$$

$$W_3\boldsymbol{\sigma}^* = J_1\dot{\Psi}\left\{\boldsymbol{\omega} - \frac{1}{2}[\boldsymbol{\omega}_e + \boldsymbol{q}_{e_v}]\right\} \tag{22}$$

where $\boldsymbol{\sigma}^* \in \mathbb{R}^{3n}$ comprises the $3n$ parameters of the J_1 matrix. Note that the regressor matrix W_2 does not contain any $\dot{\Psi}$ terms. By substituting Eqs. (20–22) into Eq. (19), the angular velocity error dynamics are reduced to

$$\begin{aligned}\dot{\boldsymbol{\omega}}_e = &-\frac{1}{2}[q_{e_0}\boldsymbol{I} + S(\boldsymbol{q}_{e_v})]\boldsymbol{\omega}_e - J^{-1}\beta\boldsymbol{q}_{e_v} - J^{-1}k_v\boldsymbol{\omega}_e\\ &+ \frac{1}{2}J^{-1}J_1\dot{\Psi}[\boldsymbol{\omega}_e + \boldsymbol{q}_{e_v}]\\ &+ J^{-1}(\boldsymbol{u} + \beta\boldsymbol{q}_{e_v} + k_v\boldsymbol{\omega}_e + W_1\boldsymbol{\theta}^* + (W_2 + W_3)\boldsymbol{\sigma}^*)\end{aligned} \tag{23}$$

Because terms involving $\boldsymbol{\theta}^*$ and $\boldsymbol{\sigma}^*$ are unknown and cannot be directly canceled by $\boldsymbol{u}$, the control is designed using parameter estimates $\hat{\boldsymbol{\theta}}$ and $\hat{\boldsymbol{\sigma}}$. That is,

$$\boldsymbol{u} = -\beta\boldsymbol{q}_{e_v} - k_v\boldsymbol{\omega}_e - W_1\hat{\boldsymbol{\theta}} - [W_2 + W_3]\hat{\boldsymbol{\sigma}} \tag{24}$$

with parameter estimation update laws

$$\dot{\hat{\boldsymbol{\theta}}} = \gamma_1 W_1^T[\boldsymbol{\omega}_e + \boldsymbol{q}_{e_v}] \tag{25}$$

$$\dot{\hat{\boldsymbol{\sigma}}} = \gamma_2[W_2 + W_3]^T[\boldsymbol{\omega}_e + \boldsymbol{q}_{e_v}] \tag{26}$$

where k_v, β, γ_1, $\gamma_2 > 0$ are any scalar constants. Finally, by substituting Eq. (24) into Eq. (23), the following closed-loop tracking error dynamics are obtained:

$$\begin{aligned}\dot{\boldsymbol{\omega}}_e = &-\frac{1}{2}[q_{e_0}I + S(\boldsymbol{q}_{e_v})]\boldsymbol{\omega}_e - J^{-1}\beta\boldsymbol{q}_{e_v} - J^{-1}k_v\boldsymbol{\omega}_e\\ &+ \frac{1}{2}J^{-1}J_1\dot{\Psi}[\boldsymbol{\omega}_e + \boldsymbol{q}_{e_v}]\\ &+ J^{-1}(-W_1\tilde{\boldsymbol{\theta}} - (W_2 + W_3)\tilde{\boldsymbol{\sigma}})\end{aligned} \tag{27}$$

where $\tilde{\boldsymbol{\theta}} = \hat{\boldsymbol{\theta}} - \boldsymbol{\theta}^*$ and $\tilde{\boldsymbol{\sigma}} = \hat{\boldsymbol{\sigma}} - \boldsymbol{\sigma}^*$ are the estimation error quantities. The main result is now stated in the theorem that follows.

Theorem 1: Consider the attitude-tracking error system of Eqs. (5) and (6) with a time- and/or state-dependent inertia matrix J given by Eq. (7) with derivative Eq. (10). Suppose further that J_1 and J_0 are unknown. Then, the adaptive control law Eq. (24), along with the parameter estimation update laws (25) and (26) guarantee asymptotic convergence of the tracking error signals $\lim_{t\to\infty}[\boldsymbol{q}_{e_v}(t), \boldsymbol{\omega}_e(t)] = 0$ for any initial condition $[\boldsymbol{q}(0), \boldsymbol{\omega}(0)]$ and all reference trajectories $[\boldsymbol{q}_r(t), \boldsymbol{\omega}_r(t)]$, with smooth and bounded $\boldsymbol{\omega}_r(t)$, while ensuring boundedness for all closed-loop signals.

Proof: Consider the following positive semidefinite Lyapunov-like function:

$$V = \frac{1}{2}(\boldsymbol{\omega}_e + \boldsymbol{q}_{e_v})^T J(\boldsymbol{\omega}_e + \boldsymbol{q}_{e_v}) + (\beta + k_v)(\boldsymbol{q}_{e_v}^T \boldsymbol{q}_{e_v} + (q_{e_0} - 1)^2) + \frac{1}{2\gamma_1}\tilde{\boldsymbol{\theta}}^T\tilde{\boldsymbol{\theta}} + \frac{1}{2\gamma_2}\tilde{\boldsymbol{\sigma}}^T\tilde{\boldsymbol{\sigma}} \tag{28}$$

Taking the derivative of V and using the closed-loop system dynamics in Eqs. (5) and (27) along with the identity $(\boldsymbol{\omega}_e + \boldsymbol{q}_{e_v})^T(\boldsymbol{q}_{e_v} \times \boldsymbol{\omega}_e) = 0$ and making appropriate cancellations leads to

$$\begin{aligned}
\dot{V} &= (\boldsymbol{\omega}_e + \boldsymbol{q}_{e_v})^T\left(-\frac{1}{2}J_1\dot{\Psi}[\boldsymbol{\omega}_e + \boldsymbol{q}_{e_v}] + J(\dot{\boldsymbol{\omega}}_e + \dot{\boldsymbol{q}}_{e_v})\right) \\
&\quad - 2(\beta + k_v)\dot{q}_{e_0} + \frac{1}{\gamma_1}\tilde{\boldsymbol{\theta}}^T\dot{\hat{\boldsymbol{\theta}}} + \frac{1}{\gamma_2}\tilde{\boldsymbol{\sigma}}^T\dot{\hat{\boldsymbol{\sigma}}} \\
&= (\boldsymbol{\omega}_e + \boldsymbol{q}_{e_v})^T(-\beta\boldsymbol{q}_{e_v} - k_v\boldsymbol{\omega}_e - W_1\tilde{\boldsymbol{\theta}} - (W_2 + W_3)\tilde{\boldsymbol{\sigma}}) \\
&\quad + (\beta + k_v)\boldsymbol{q}_{e_v}^T\boldsymbol{\omega}_e + \frac{1}{\gamma_1}\tilde{\boldsymbol{\theta}}^T\dot{\hat{\boldsymbol{\theta}}} + \frac{1}{\gamma_2}\tilde{\boldsymbol{\sigma}}^T\dot{\hat{\boldsymbol{\sigma}}} \\
&= -k_v\|\boldsymbol{\omega}_e\|^2 - \beta\|\boldsymbol{q}_{e_v}\|^2 + \tilde{\boldsymbol{\theta}}^T\left(\frac{1}{\gamma_1}\dot{\hat{\boldsymbol{\theta}}} - W_1^T(\boldsymbol{\omega}_e + \boldsymbol{q}_{e_v})\right) \\
&\quad + \tilde{\boldsymbol{\sigma}}^T\left(\frac{1}{\gamma_2}\dot{\hat{\boldsymbol{\sigma}}} - (W_2 + W_3)^T(\boldsymbol{\omega}_e + \boldsymbol{q}_{e_v})\right)
\end{aligned}$$

By selecting $\dot{\hat{\boldsymbol{\theta}}}$ and $\dot{\hat{\boldsymbol{\sigma}}}$ according to Eqs. (25) and (26), one obtains

$$\dot{V} = -k_v\|\boldsymbol{\omega}_e\|^2 - \beta\|\boldsymbol{q}_{e_v}\|^2$$

which is negative semidefinite. Since $V \geq 0$ and $\dot{V} \leq 0$, V is a monotonic function indicating that $V(t) \leq V(0)$. Consequently, all closed-loop signals are bounded. Furthermore,

$$\int_0^t \dot{V}(t)\,\mathrm{d}t$$

exists and is finite, which implies that $\boldsymbol{q}_{e_v}$, $\boldsymbol{\omega}_e$, $\in \mathcal{L}_2 \cap \mathcal{L}_\infty$ and, consequently, from Eqs. (5) and (27), it follows that $\dot{\boldsymbol{q}}_{e_v}, \dot{\boldsymbol{\omega}}_e, \in \mathcal{L}_\infty$. Invoking Barbalat's lemma leads to $\lim_{t\to\infty}[\boldsymbol{q}_{e_v}(t), \boldsymbol{\omega}_e(t)] = 0$.

The parameter update laws in Eqs. (25) and (26) suffer from the drawback that the parameters $\hat{\boldsymbol{\theta}}$ and $\hat{\boldsymbol{\sigma}}$ can drift arbitrarily away from their respective true values. However, if the true parameters are bounded by a known scalar constant, then the estimates can also be constrained to evolve within a bounded convex set with known bound. This can be accomplished by modifying the parameter update laws by using a smooth projection algorithm [20,21].

A suitable modification for the update law for $\hat{\boldsymbol{\theta}}$ is discussed next. To this end, define two convex sets

$$\Omega_{\theta^*} \triangleq \{\boldsymbol{\theta}^* \in \mathbb{R}^6 | \|\boldsymbol{\theta}^*\|^2 < \epsilon_1\}, \qquad \Omega_{\hat{\theta}} \triangleq \{\hat{\boldsymbol{\theta}} \in \mathbb{R}^6 | \|\hat{\boldsymbol{\theta}}\|^2 < \epsilon_1 + \delta_1\} \tag{29}$$

for known $\epsilon_1 > 0$ and $\delta_1 > 0$. Consider the following smooth projection scheme for $\hat{\boldsymbol{\theta}}$:

$$\dot{\hat{\boldsymbol{\theta}}} = \mathrm{Proj}(\hat{\boldsymbol{\theta}}, \Phi); \qquad \Phi \triangleq W_1^T[\boldsymbol{\omega}_e + \boldsymbol{q}_{e_v}] \tag{30}$$

where

$$\mathrm{Proj}(\hat{\boldsymbol{\theta}}, \Phi) \triangleq \begin{cases} \gamma_1\Phi & \text{if 1) } \|\hat{\boldsymbol{\theta}}\|^2 < \epsilon_1 \text{ or} \\ & \text{if 2) } \|\hat{\boldsymbol{\theta}}\|^2 \geq \epsilon_1 \text{ and } \Phi^T\hat{\boldsymbol{\theta}} \leq 0 \\ \gamma_1\left(\Phi - \frac{(\|\hat{\boldsymbol{\theta}}\|^2 - \epsilon_1)\Phi^T\hat{\boldsymbol{\theta}}}{\delta_1\|\hat{\boldsymbol{\theta}}\|^2}\hat{\boldsymbol{\theta}}\right) & \text{if 3) } \|\hat{\boldsymbol{\theta}}\|^2 \geq \epsilon_1 \text{ and } \Phi^T\hat{\boldsymbol{\theta}} > 0 \end{cases} \tag{31}$$

The projection operator $\mathrm{Proj}(\hat{\boldsymbol{\theta}}, \Phi)$ is locally Lipschitz [21] in $(\hat{\boldsymbol{\theta}}, \Phi)$ and switches smoothly between cases 1–3. Note that this update law is exactly equal to Eq. (25) in cases 1 and 2. Furthermore, it is straightforward to show that $\mathrm{Proj}(\hat{\boldsymbol{\theta}}, \Phi)$ satisfies

$$\hat{\boldsymbol{\theta}}(0) \in \Omega_{\hat{\theta}} \Rightarrow \hat{\boldsymbol{\theta}}(t) \in \Omega_{\hat{\theta}} \tag{32}$$

for all $t \geq 0$. In case 1, Eq. (32) readily holds because $\hat{\boldsymbol{\theta}} \in \Omega_{\theta^*}$ and $\Omega_{\theta^*} \subset \Omega_{\hat{\theta}}$. In case 2, $\|\hat{\boldsymbol{\theta}}\|^2$ evolves according to

$$\frac{\mathrm{d}}{\mathrm{d}t}\|\hat{\boldsymbol{\theta}}\|^2 = 2\hat{\boldsymbol{\theta}}^T\dot{\hat{\boldsymbol{\theta}}} = 2\gamma_1\hat{\boldsymbol{\theta}}^T\Phi$$

which is trivially negative semidefinite by the conditions stated in case 2. Consequently, the estimates approach the origin. Finally, for case 3,

$$\frac{\mathrm{d}}{\mathrm{d}t}\|\hat{\boldsymbol{\theta}}\|^2 = 2\hat{\boldsymbol{\theta}}^T\dot{\hat{\boldsymbol{\theta}}} = 2\frac{\gamma_1}{\delta}\hat{\boldsymbol{\theta}}^T\Phi(\delta_1 + \epsilon_1 - \|\hat{\boldsymbol{\theta}}\|^2)$$

which decreases when $\|\hat{\boldsymbol{\theta}}\|^2 > \epsilon_1 + \delta_1$, increases if $\|\hat{\boldsymbol{\theta}}\|^2 < \epsilon_1 + \delta_1$, and is exactly zero when $\|\hat{\boldsymbol{\theta}}\|^2 = \epsilon_1 + \delta_1$. Thus, the adaptation law in Eq. (30) ensures that $\hat{\boldsymbol{\theta}}(t)$ remains in the set $\Omega_{\hat{\sigma}}$.

A smooth projection parameter update law for $\hat{\boldsymbol{\sigma}}$ is synthesized in a fashion identical to $\hat{\boldsymbol{\theta}}$. Assuming that $\|\boldsymbol{\sigma}^*(t)\|$ is bounded by an a priori available constant value, define two convex sets

$$\begin{aligned}
\Omega_{\sigma^*} &\triangleq \{\boldsymbol{\sigma}^* \in \mathbb{R}^{3n} | \|\boldsymbol{\sigma}^*\|^2 < \epsilon_2\}, \\
\Omega_{\hat{\sigma}} &\triangleq \{\hat{\boldsymbol{\sigma}} \in \mathbb{R}^{3n} | \|\hat{\boldsymbol{\sigma}}\|^2 < \epsilon_2 + \delta_2\}
\end{aligned} \tag{33}$$

for known $\epsilon_2 > 0$ and $\delta_2 > 0$. The smooth projection scheme for $\hat{\boldsymbol{\sigma}}$ is then given by

$$\dot{\hat{\boldsymbol{\sigma}}} = \mathrm{Proj}(\hat{\boldsymbol{\sigma}}, \Gamma); \qquad \Gamma \triangleq [W_2 + W_3]^T[\boldsymbol{\omega}_e + \boldsymbol{q}_{e_v}] \tag{34}$$

where

$$\mathrm{Proj}(\hat{\boldsymbol{\sigma}}, \Gamma) \triangleq \begin{cases} \gamma_2\Gamma & \text{if 1) } \|\hat{\boldsymbol{\sigma}}\|^2 < \epsilon_2 \text{ or} \\ & \text{if 2) } \|\hat{\boldsymbol{\sigma}}\|^2 \geq \epsilon_2 \text{ and } \Gamma^T\hat{\boldsymbol{\sigma}} \leq 0 \\ \gamma_2\left(\Gamma - \frac{(\|\hat{\boldsymbol{\sigma}}\|^2 - \epsilon_2)\Gamma^T\hat{\boldsymbol{\sigma}}}{\delta_2\|\hat{\boldsymbol{\sigma}}\|^2}\hat{\boldsymbol{\sigma}}\right) & \text{if 3) } \|\hat{\boldsymbol{\sigma}}\|^2 \geq \epsilon_2 \text{ and } \Gamma^T\hat{\boldsymbol{\sigma}} > 0 \end{cases} \tag{35}$$

which is similarly locally Lipschitz and satisfies $\hat{\boldsymbol{\sigma}}(0) \in \Omega_{\hat{\sigma}} \Rightarrow \hat{\boldsymbol{\sigma}}(t) \in \Omega_{\hat{\sigma}}$.

Theorem 2: Suppose that $\boldsymbol{\theta}^* \in \Omega_{\theta^*}, \boldsymbol{\sigma}^* \in \Omega_{\sigma^*}$, and inertia matrix J in Eq. (7) is time and/or state dependent with dynamics given by Eq. (10) and unknown J_0 and J_1. Then, the adaptive control law (24), together with smooth projection update laws (30) and (34) and initial conditions $\hat{\boldsymbol{\theta}}(0) \in \Omega_{\hat{\theta}}$ and $\hat{\boldsymbol{\sigma}}(0) \in \Omega_{\hat{\sigma}}$, stabilizes the system of Eqs. (5) and (6) while ensuring boundedness for all closed-loop signals and asymptotic convergence of the tracking error $\lim_{t\to\infty}[\boldsymbol{q}_{e_v}(t), \boldsymbol{\omega}_e(t)] = 0$ for all initial conditions $[\boldsymbol{q}(0), \boldsymbol{\omega}(0)]$ and any reference trajectory $[\boldsymbol{q}_r(t), \boldsymbol{\omega}_r(t)]$ with $\boldsymbol{\omega}_r$ smooth and bounded.

Proof: Consider again the Lyapunov function V defined previously in Eq. (28). Evaluating $\dot{V}$ along the closed-loop system trajectories yields

$$\dot{V} = -k_v\|\boldsymbol{\omega}_e\|^2 - \beta\|\boldsymbol{q}_{e_v}\|^2 + \frac{1}{\gamma_1}\tilde{\boldsymbol{\theta}}^T(\dot{\hat{\boldsymbol{\theta}}} - \gamma_1\Phi) + \frac{1}{\gamma_2}\tilde{\boldsymbol{\sigma}}^T(\dot{\hat{\boldsymbol{\sigma}}} - \gamma_2\Gamma)$$
$$= -k_v\|\boldsymbol{\omega}_e\|^2 - \beta\|\boldsymbol{q}_{e_v}\|^2 + \dot{V}_2 + \dot{V}_3$$

which is negative semidefinite if

$$\dot{V}_2 = \tilde{\boldsymbol{\theta}}^T(\dot{\hat{\boldsymbol{\theta}}} - \gamma_1\Phi) \le 0, \qquad \dot{V}_3 = \tilde{\boldsymbol{\sigma}}^T(\dot{\hat{\boldsymbol{\sigma}}} - \gamma_2\Gamma) \le 0$$

If $\dot{\hat{\boldsymbol{\theta}}}$ is prescribed according to the adaptation law (30), $\dot{V}_2 \le 0$ is trivially satisfied for cases 1 and 2. For case 3,

$$\tilde{\boldsymbol{\theta}}^T(\dot{\hat{\boldsymbol{\theta}}} - \gamma_1\Phi) = \tilde{\boldsymbol{\theta}}^T\left(\gamma_1\left(\Phi - \frac{(\|\hat{\boldsymbol{\theta}}\|^2 - \epsilon_1)\Phi^T\hat{\boldsymbol{\theta}}}{\delta_1\|\hat{\boldsymbol{\theta}}\|^2}\hat{\boldsymbol{\theta}}\right) - \gamma_1\Phi\right)$$
$$= -\gamma_1\left(\frac{(\|\hat{\boldsymbol{\theta}}\|^2 - \epsilon_1)\Phi^T\hat{\boldsymbol{\theta}}}{\delta_1\|\hat{\boldsymbol{\theta}}\|^2}\tilde{\boldsymbol{\theta}}^T\hat{\boldsymbol{\theta}}\right) \le 0$$

which is true because $\tilde{\boldsymbol{\theta}}^T\hat{\boldsymbol{\theta}} = \|\hat{\boldsymbol{\theta}}\|^2 - \boldsymbol{\theta}^{*T}\hat{\boldsymbol{\theta}} \ge 0$ when $\|\hat{\boldsymbol{\theta}}\|^2 \ge \epsilon_1$. Therefore,

$$\dot{V}_2 = \begin{cases} 0 & \text{in case 1 and case 2} \\ -\gamma_1\left(\frac{(\|\hat{\boldsymbol{\theta}}\|^2 - \epsilon_1)\Phi^T\hat{\boldsymbol{\theta}}}{\delta_1\|\hat{\boldsymbol{\theta}}\|^2}\tilde{\boldsymbol{\theta}}^T\hat{\boldsymbol{\theta}}\right) \le 0 & \text{in case 3} \end{cases} \tag{36}$$

from which it follows that $\dot{V}_2 \le 0$. Similarly, it can be shown that $\dot{V}_3 \le 0$, from which it follows that $\dot{V} \le 0$. As shown in the proof for Proposition 1, $\boldsymbol{q}_{e_v}, \boldsymbol{\omega}_e, \in \mathcal{L}_2 \cap \mathcal{L}_\infty$ and $\dot{\boldsymbol{q}}_{e_v}, \dot{\boldsymbol{\omega}}_e, \in \mathcal{L}_\infty$ can be readily asserted. Furthermore, $\dot{V}$ is uniformly continuous because $\dot{V}_2$ and $\dot{V}_3$ are Lipschitz continuous at the boundaries between their respective cases 1–3. Thus, from an application of Barbalat's lemma, it follows then that $\lim_{t\to\infty}[\boldsymbol{q}_{e_v}(t), \boldsymbol{\omega}_e(t)] = 0$.

IV. Adaptive Attitude-Tracking Control for Unknown Inertia with Input Dependency

In this section, the adaptive controller is extended to handle fuel loss compensation, wherein the spacecraft inertia matrix has an explicit control input dependency. After careful examination and judicious rearrangement of terms, the control law given by Eq. (24) can be expressed in terms of the control-dependent inertia matrix in Eq. (17) in the following manner:

$$\boldsymbol{u} = \boldsymbol{\tau} - \|\boldsymbol{u}\|\hat{J}_1\Omega \tag{37}$$

where $\hat{J}_1$ is the estimate of matrix J_1 and

$$\boldsymbol{\tau} = -\beta\boldsymbol{q}_{e_v} - k_v\boldsymbol{\omega}_e - W_1\hat{\boldsymbol{\theta}} - W_2\hat{\boldsymbol{\sigma}} \tag{38}$$

$$\Omega = \boldsymbol{\omega} - \frac{1}{2}[\boldsymbol{\omega}_e + \boldsymbol{q}_{e_v}] \tag{39}$$

The second term in Eq. (37) is obtained by recognizing that $W_3\boldsymbol{\sigma}^* = J_1\Psi\Omega$ and using Eq. (17) to express $W_3\hat{\boldsymbol{\sigma}} = \|\boldsymbol{u}\|\hat{J}_1\Omega$. Note that, Ω can be equivalently stated as

$$\Omega = \frac{1}{2}\boldsymbol{\omega}_e + \boldsymbol{\omega}_{rB} - \frac{1}{2}\boldsymbol{q}_{e_v} \tag{40}$$

where $\boldsymbol{\omega}_{rB} = C(\boldsymbol{q}_r)\boldsymbol{\omega}_r$. To obtain an implementable expression for $\boldsymbol{u}$, Eq. (37) is examined further. From Eq. (37), the following expression is readily obtained for $\|\boldsymbol{u}\|^2$:

$$\|\boldsymbol{u}\|^2 = \|\boldsymbol{\tau}\|^2 - 2\|\boldsymbol{u}\|\boldsymbol{\tau}^T\hat{J}_1\Omega + \|\boldsymbol{u}\|^2\|\hat{J}_1\Omega\|^2 \tag{41}$$

which can be rearranged to obtain

$$\|\boldsymbol{u}\|^2(1 - \|\hat{J}_1\Omega\|^2) + 2\|\boldsymbol{u}\|\boldsymbol{\tau}^T\hat{J}_1\Omega - \|\boldsymbol{\tau}\|^2 = 0 \tag{42}$$

Observe that Eq. (42) is a simple quadratic equation in $\|\boldsymbol{u}\|$. Suppose it is ensured that

$$\|\hat{J}_1\Omega\| < 1 \tag{43}$$

then $(1 - \|\hat{J}_1\Omega\|^2) > 0$ for all $t \ge 0$ and Eq. (42) has only the following nonnegative solution for $\|\boldsymbol{u}\|$:

$$\|\boldsymbol{u}\| = \frac{-2\boldsymbol{\tau}^T\hat{J}_1\Omega + \sqrt{4(\boldsymbol{\tau}^T\hat{J}_1\Omega)^2 + 4(1 - \|\hat{J}_1\Omega\|^2)\|\boldsymbol{\tau}\|^2}}{2(1 - \|\hat{J}_1\Omega\|^2)} \tag{44}$$

which is nonnegative and bounded if Eq. (43) holds for all $t \ge 0$. Hence, the control input expression in Eq. (37) together with Eq. (44) is bounded and implementable for $t \ge 0$ as long as the inequality in Eq. (43) is satisfied. Next, to ensure that Eq. (43) is satisfied for all time, observe that

$$\|\hat{J}_1\Omega\| \le \|\hat{J}_1\|\|\Omega\|$$
$$\le \|\hat{J}_1\|\left\|\frac{\boldsymbol{\omega}_e}{2} + \boldsymbol{\omega}_{rB} - \frac{\boldsymbol{q}_{e_v}}{2}\right\|$$
$$\le \|\hat{J}_1\|\left(\frac{\|\boldsymbol{\omega}_e\|}{2} + \omega_B + \frac{1}{2}\right) \tag{45}$$

where the bounds $\omega_B = \sup_{t\ge0}\|\boldsymbol{\omega}_{rB}\|$ and $\|\boldsymbol{q}_{e_v}\| \le 1$ have been employed to obtain Eq. (45). Using the two-norm bound $\|\hat{J}_1\| \le 3_{t\ge0}(\max_{i,j}|\hat{J}_{1_{ij}}(t)|)$, where $\hat{J}_{1_{ij}}$ is the i, jth entry of matrix J_1, and invoking the constraint $\|\hat{\sigma}_i\| \le \|\hat{\boldsymbol{\sigma}}\| \le \sqrt{\epsilon_2 + \delta_2}$ $\forall$ $i = 1, 2, 3$ as long as $\hat{\boldsymbol{\sigma}}$ is updated according to the smooth projection algorithm of Eq. (34), Eq. (45) can be expressed as

$$\|\hat{J}_1\Omega\| \le 3\sqrt{\epsilon_2 + \delta_2}\left(\frac{\|\boldsymbol{\omega}_e\|}{2} + \boldsymbol{\omega}_B + \frac{1}{2}\right) \tag{46}$$

Upper bounding the right-hand side of Eq. (46) by unity leads to the following conservative upper bound on the norm of $\boldsymbol{\omega}_e$:

$$\|\boldsymbol{\omega}_e(t)\| < \zeta^*; \qquad \zeta^* = 2\left(\frac{1}{3\sqrt{\epsilon_2 + \delta_2}} - \omega_B - \frac{1}{2}\right) \tag{47}$$

where ϵ_2 and δ_2 are such that $\zeta^* > 0$ for all $t \ge 0$. Thus, if $\boldsymbol{\omega}_e$ is upper bounded according to Eq. (47), then $\|\hat{J}_1\Omega\| < 1$ and the control input in Eq. (37) along with Eq. (44) is nonnegative and bounded for all $t \ge 0$.

Theorem 3: Consider the attitude-tracking error system of Eqs. (5) and (6) with an input-dependent inertia matrix J that evolves according to Eq. (17) and components J_1 and J_0 being unknown. Suppose the true parameter values $\boldsymbol{\theta}^*$ and $\boldsymbol{\sigma}^*$ are such that

$$\boldsymbol{\theta}^* \in \Omega_{\theta^*}; \qquad \boldsymbol{\sigma}^* \in \Omega_{\sigma^*}, \tag{48}$$

and the inertia matrix J is described by known values $\lambda_{\min}$ and $\lambda_{\max}$, such that

$$\lambda_{\min} = \inf_{\substack{i=1,2,3 \\ t\ge0}} \lambda_i(t); \qquad \lambda_{\max} = \sup_{\substack{i=1,2,3 \\ t\ge0}} \lambda_i(t) \tag{49}$$

where $\lambda_i(t)$ denotes the ith (potentially) time-varying eigenvalue of J pointwise with time. Furthermore, suppose the initial conditions satisfy

$$(\|\boldsymbol{\omega}_e(0)\| + 1)^2$$
$$< \frac{2}{\lambda_{\max}}\left[\frac{\lambda_{\min}}{2}(\zeta^* - 1)^2 - \frac{\lambda_{\min}}{2} - 4(\beta + k_v) - \frac{\tilde{\theta}_{\max}}{2\gamma_1} - \frac{\tilde{\sigma}_{\max}}{2\gamma_2}\right] \tag{50}$$

where ζ^* is given by Eq. (47) and selected such that $\zeta^* > 1$, $\tilde{\theta}_{\max} = (\sqrt{\epsilon_1 + \delta_1} + \sqrt{\epsilon_1})^2$ and $\tilde{\sigma}_{\max} = (\sqrt{\epsilon_2 + \delta_2} + \sqrt{\epsilon_2})^2$. In addition, the right-hand side of the preceding inequality satisfies

$$\left[\frac{\lambda_{\min}}{2}(\zeta^* - 1)^2 - \frac{\lambda_{\min}}{2} - 4(\beta + k_v) - \frac{\tilde{\theta}_{\max}}{2\gamma_1} - \frac{\tilde{\sigma}_{\max}}{2\gamma_2}\right] > 0 \quad (51)$$

Then, the adaptive control law in the form of Eq. (37) with Eq. (44) is nonsingular for all $t \geq 0$ and, along with smooth projection-based parameter update laws (30–34) and initial conditions $\hat{\boldsymbol{\theta}}(0) \in \Omega_{\hat{\theta}}$ and $\hat{\boldsymbol{\sigma}}(0) \in \Omega_{\hat{\sigma}}$, guarantees asymptotic convergence of the tracking error signals $\lim_{t\to\infty}[\boldsymbol{q}_{e_v}(t), \boldsymbol{\omega}_e(t)] = 0$ for all bounded and smooth reference trajectories $[\boldsymbol{q}_r(t), \boldsymbol{\omega}_r(t)]$, while ensuring boundedness for all closed-loop signals for all $t \geq 0$.

Proof: First and foremost, it is shown that the adaptive control input given by Eqs. (37) and (44) is nonsingular for all $t \geq 0$. Consider again the positive semidefinite function V in Eq. (28). As outlined in the proof for Theorem 1, evaluating $\dot{V}$ along the closed-loop system trajectories (5) and (27) with parameter update laws Eqs. (30) and (34) yields $\dot{V} \leq 0$. Thus, V is a monotonic function and satisfies $V(t) \leq V(0)$. For notational convenience in the analysis that follows, V in Eq. (28) is written as

$$V = \frac{1}{2}(\boldsymbol{\omega}_e + \boldsymbol{q}_{e_v})^T J(\boldsymbol{\omega}_e + \boldsymbol{q}_{e_v}) + \tilde{V}$$

where the positive semidefinite function $\tilde{V}$ is simply

$$\tilde{V} = (\beta + k_v)(\boldsymbol{q}_{e_v}^T \boldsymbol{q}_{e_v} + (q_{e_0} - 1)^2) + \frac{1}{2\gamma_1}\|\tilde{\boldsymbol{\theta}}\|^2 + \frac{1}{2\gamma_2}\|\tilde{\boldsymbol{\sigma}}\|^2$$

Then, using the Rayleigh–Ritz inequality coupled with the monotonicity of V, one can write

$$\frac{\lambda_{\min}}{2}\|\boldsymbol{\omega}_e + \boldsymbol{q}_{e_v}\|^2 + \tilde{V} \leq V(t) \leq V(0) \quad (52)$$

Following through with some minor algebra and rearrangement of terms in Eq. (52) leads to

$$\begin{aligned}\frac{\lambda_{\min}}{2}\|\boldsymbol{\omega}_e\|^2 + \frac{\lambda_{\min}}{2}\|\boldsymbol{q}_{e_v}\|^2 + \tilde{V} &\leq V(0) - \lambda_{\min}\boldsymbol{\omega}_e^T \boldsymbol{q}_e \\ &\leq V(0) + \lambda_{\min}\|\boldsymbol{\omega}_e\| \end{aligned} \quad (53)$$

Adding the terms $-\lambda_{\min}\|\boldsymbol{\omega}_e\| + \lambda_{\min}/2$ on both sides of the inequality in Eq. (53) and following through with completion of squares yields

$$\frac{\lambda_{\min}}{2}(\|\boldsymbol{\omega}_e\| - 1)^2 + \frac{\lambda_{\min}}{2}\|\boldsymbol{q}_{e_v}\|^2 + \tilde{V} \leq V(0) + \frac{\lambda_{\min}}{2} \quad (54)$$

Next, using again the Rayleigh–Ritz inequality and implementing the upper bound on $\|\boldsymbol{\omega}_e(0)\|$ stated in Eq. (50), $V(0)$ can be upper bounded as follows:

$$\begin{aligned} V(0) &\leq \frac{\lambda_{\max}}{2}\|\boldsymbol{\omega}_e(0) + \boldsymbol{q}_{e_v}(0)\|^2 + 2(\beta + k_v)(1 - q_{e_0}) \\ &\quad + \frac{1}{2\gamma_1}\|\tilde{\boldsymbol{\theta}}\|^2 + \frac{1}{2\gamma_2}\frac{\|\tilde{\boldsymbol{\sigma}}\|^2}{} \\ &\leq \frac{\lambda_{\max}}{2}(\|\boldsymbol{\omega}_e(0)\| + \|\boldsymbol{q}_{e_v}(0)\|)^2 + 4(\beta + k_v) \\ &\quad + \frac{1}{2\gamma_1}(\|\hat{\boldsymbol{\theta}}\| + \|\boldsymbol{\theta}^*\|)^2 + \frac{1}{2\gamma_2}(\|\hat{\boldsymbol{\sigma}}\| + \|\boldsymbol{\sigma}^*\|)^2 \\ &\leq \frac{\lambda_{\max}}{2}(\|\boldsymbol{\omega}_e(0)\| + 1)^2 + 4(\beta + k_v) + \frac{\tilde{\theta}_{\max}}{2\gamma_1} + \frac{\tilde{\sigma}_{\max}}{2\gamma_2} \\ &< \frac{\lambda_{\min}}{2}(\zeta^* - 1)^2 - \frac{\lambda_{\min}}{2} \end{aligned} \quad (55)$$

Using Eq. (55) as the upper bound for $V(0)$ in Eq. (54) gives

$$\frac{\lambda_{\min}}{2}(\|\boldsymbol{\omega}_e\| - 1)^2 + \frac{\lambda_{\min}}{2}\|\boldsymbol{q}_{e_v}\|^2 + \tilde{V} < \frac{\lambda_{\min}}{2}(\zeta^* - 1)^2 \quad (56)$$

from which it readily follows that $(\|\boldsymbol{\omega}_e\| - 1)^2 < (\zeta^* - 1)^2$ and, since $\zeta^* > 1$, $\|\boldsymbol{\omega}_e(t)\| < \zeta^*$ for all $t \geq 0$, ensuring nonsingularity of the control in Eq. (37) with $\|\boldsymbol{u}\|$ prescribed according to Eq. (44). The remainder of the proof showing asymptotic convergence of error signals and boundedness of closed-loop signals follows exactly according to the proof for Theorem 2.

A few pertinent remarks and observations are now made about Theorem 3:

1) It is important to remark that the smooth projection algorithm of Eq. (34) is crucial for ensuring that the adaptive control solution in Eq. (37) with $\|\boldsymbol{u}\|$ given by Eq. (44) is uniformly bounded when dealing with inertia variations due to control torque-induced fuel expenditure. Without this assumption, no assurance can be provided that Eq. (42) will yield a nonsingular solution for $\|\boldsymbol{u}\|$.

2) For the specific case of inertia variations due to fuel loss, since $\|J(t)\| \leq \|J_0\|$, knowing $\lambda_{\max}$ is equivalent to having knowledge of the maximum eigenvalue of J_0.

3) From a practical standpoint, the minimum eigenvalue of $J(t)$ at any time t is larger than the minimum eigenvalue at the completion of the mission, or when the fuel mass has been entirely expended. Thus, having knowledge of $\lambda_{\min}$ is equivalent to knowing the minimum eigenvalue of the inertia matrix associated with the dry mass of the spacecraft.

4) The practical implication of requiring $\zeta^* > 1$ to ensure control implementability needs further examination. For convenience, the expression for ζ^* from Eq. (47) is restated as

$$\zeta^* = 2\left(\frac{1}{3\sqrt{\epsilon_2 + \delta_2}} - \omega_B - \frac{1}{2}\right)$$

Recall that $\sqrt{\epsilon_2 + \delta_2}$ is the upper bound on estimates of J_1, whereas ω_B is the upper bound of the reference velocity. Thus, if ϵ_2 and δ_2 are small and if ω_B is not impractically large, then $\zeta^* > 1$ can be readily satisfied. Note that this condition is a sufficient condition and may be potentially overly conservative. It is, of course, possible for the control law to be implementable even when this condition is not satisfied.

5) Finally, a few observations are in order regarding the initial condition requirement of Eq. (50) to ensure control implementability. As will be shown in the numerical simulations that follow, the initial condition requirement is practically quite lenient and permits a vast range of reference trajectories and initial conditions. Restated here for convenience, it is observed that the right-hand side of the inequality (50) is essentially a function of the spacecraft inertia matrix properties and the reference trajectory, as well as the gains β, k_v, γ_1, γ_2:

$$\begin{aligned}&(\|\boldsymbol{\omega}_e(0)\| + 1)^2 \\ &\quad < \frac{2}{\lambda_{\max}}\left[\frac{\lambda_{\min}}{2}(\zeta^* - 1)^2 - \frac{\lambda_{\min}}{2} - 4(\beta + k_v) - \frac{\tilde{\theta}_{\max}}{2\gamma_1} - \frac{\tilde{\sigma}_{\max}}{2\gamma_2}\right]\end{aligned}$$

The last three negative-definite terms on the right-hand side of this inequality can be driven close to zero through appropriate selection of gain terms. Then, if $\lambda_{\min}[(\zeta^* - 1)^2 - 1]/2$ is large enough to overcome the offending negative terms, a large range of $\boldsymbol{\omega}_e(0)$ is easily accommodated in Eq. (50). Again, it is noted that the restriction on the initial condition is a sufficient condition only, and that the control may be implementable even if Eq. (50) is not satisfied.

V. Numerical Simulations

To show the performance characteristics of the proposed adaptive control, numerical simulations are conducted. The error tracking capabilities are compared to a high-performance noncertainty equivalence-based adaptive control [3] that does not account for inertia variations. The control protocol in [3] is referred to as "comparison" in the subsequent simulations and is listed as

$$\boldsymbol{u}_c = -W_c(\hat{\boldsymbol{\theta}} + \boldsymbol{\beta}_c) - \gamma W_f W_f^T[k_p(\boldsymbol{\omega}_f - \boldsymbol{q}_{e_v}) - \boldsymbol{\omega}_e] \quad (57)$$

$$\dot{\hat{\boldsymbol{\theta}}}_c = \gamma W_f^T[(\alpha + k_w)\boldsymbol{\omega}_f + k_p \boldsymbol{q}_{e_v}] - \gamma W_c^T \boldsymbol{\omega}_f \tag{58}$$

$$\boldsymbol{\beta}_c = \gamma W_f^T \boldsymbol{\omega}_f \tag{59}$$

where k_p, k_w, $\gamma > 0$ are scalar constants, $\alpha = k_p + k_w$, and the matrix W_c is given by

$$W_c \boldsymbol{\theta}^* = -S(\boldsymbol{\omega})J\boldsymbol{\omega} + J\dot{\boldsymbol{\omega}} + J(k_w \boldsymbol{\omega}_e + k_p \dot{\boldsymbol{q}}_{e_v} + \alpha k_p \boldsymbol{q}_{e_v}) \tag{60}$$

and derived for a constant J, that is, $J = J_0$. Finally, the signals W_f and $\boldsymbol{\omega}_f$ are updated using

$$\dot{\boldsymbol{\omega}}_f = -\alpha \boldsymbol{\omega}_f + \boldsymbol{\omega}_e \quad \dot{W}_f = -\alpha W_f + W_c$$

with arbitrary initial conditions $\boldsymbol{\omega}_f(0) \in \mathbb{R}^3$ and $W_f(0) \in \mathbb{R}^{3\times 6}$. The choice for this comparison controller is motivated by the fact that the non-CE adaptive control in [3] has been shown to demonstrate significantly superior tracking error convergence performance to classical CE adaptive control methods owing to its attractive manifold design in the parameter adaptation dynamics. However, as shown in subsequent simulations, despite its provable performance gains for a constant inertia matrix, the non-CE adaptive controller suffers from pointing accuracy when faced with a time-varying inertia matrix.

Two types of time-varying inertia matrices are considered. In the first example, a spacecraft undergoing sensor boom deployment is modeled. In this case, a sinusoidal mass-displacement profile is used to represent persistent mass movement of an articulated appendage. In the second example, a control input-dependent inertia matrix is simulated to highlight the benefits of the novel control methodology for fuel loss compensation. In both simulations, the true value of the inertia component J_0 is taken as

$$J_0 = \begin{bmatrix} 20 & 1.2 & 0.9 \\ 1.2 & 17 & 1.4 \\ 0.9 & 1.4 & 15 \end{bmatrix} \text{ kg-m}^2 \tag{61}$$

For the most fair comparison, the initial value of both $\hat{\boldsymbol{\theta}}$ and $\hat{\boldsymbol{\theta}}_c$ is taken as $\hat{\boldsymbol{\theta}}_c(0) = \hat{\boldsymbol{\theta}}(0) = [21.1, 1.9, 1.4, 17.8, 2.9, 15.5]^T$, whereas $\hat{\boldsymbol{\sigma}}(0) = 0$ for the proposed adaptive control law. The true values for J_1 parameters are presented separately in the sections that follow. The initial angular velocity of the spacecraft is $\boldsymbol{\omega}(0) = [0.001, 0.001, 0.002]^T$, whereas the vector component of the initial body quaternion is given by $\boldsymbol{q}_v(0) = [0.1826, 0.1826, 0.1826]^T$ with $q_0 = \sqrt{1 - 3(0.1826)^2}$. The initial reference quaternion is $\boldsymbol{q}_r(0) = [1, 0, 0, 0]^T$, which indicates that the reference and inertial frames are initially aligned. Simulations are conducted for a nonpersistently exciting (non-PE) reference trajectory. Obtained from the example provided in [3], the non-PE angular velocity profile is generated according to $\boldsymbol{\omega}_r(t) = r(t)[1, 1, 1]^T$ rad/s with $r(t)$ given by

$$r(t) = (0.3\cos(0.3t)(1 - e^{0.01t^2}) + (0.08\pi + 0.006\sin(0.3t))te^{-0.01t^2}) \tag{62}$$

To obtain a fair comparison between $\boldsymbol{u}$ and $\boldsymbol{u}_c$, the parameters k_v, β, k_p, and k_w are first tuned to yield similar controller performance for the ideal case, where J is constant and known. By selecting $\beta = 20$, $k_v = 24.5$ for $\boldsymbol{u}$, and $k_w = 0.5$, $k_p = 0.5$ for $\boldsymbol{u}_c$, and setting $\gamma = \gamma_1 = \gamma_2 = 0$, the baseline plots shown in Fig. 3 show a similar controller performance.

In subsequent simulations, only the parameter estimation tuning parameters γ, γ_1, and γ_2 are modified to obtain the best performance for both controllers, while keeping the control gains unchanged. For both the fuel loss and simulation deployment cases, plots are provided along with a discussion to highlight important features of the controller.

A. Deployable Appendage

This section presents a simulation of the adaptive control in Eq. (24) along with parameter estimation update laws (25) and (26) (without projection) for a purely time-varying inertia matrix. A spacecraft with articulating parts is modeled using Eqs. (11–13) with known quantities

$$\boldsymbol{\rho}_1(t) = 0.5[1 + \sin^2(0.1t)]\hat{\boldsymbol{b}}_1 \tag{63}$$

$$\boldsymbol{\rho}_2(t) = 0.8[1 + \sin^2(0.1t)]\hat{\boldsymbol{b}}_2 \tag{64}$$

along with unknown mass $m_1 = 1$ kg and $m_2 = 1.3$ kg. Thus, J_1 is given by $J_1 = -[1.0 \cdot I, 1.3 \cdot I]$ where I is the 3×3 identity matrix. The matrix J_0 is given by Eq. (61), with the assumption that the inertia contributions of the moving objects are already included in the calculation of J_0 in accordance with Eq. (11), or that the moving parts are treated as point masses. Figure 4 illustrates the evolution of the principal moments of inertia of this inertia matrix over a period of 400 s. The inertia matrix quantities remain positive definite and satisfy Eq. (9) throughout the simulation period.

The tuning parameters are selected to be $\gamma = 100$, $\gamma_1 = 60$, and $\gamma_2 = 200$ and are chosen in such a manner to yield a result closest to the baseline performance for each controller. Every effort was made by the authors to select the best possible tuning parameters for each control method. The results are illustrated in Figs. 5 and 6. Although the proposed controller maintains consistent closed-loop tracking-performance, the comparison controller suffers greatly due to the persistent variations in the input-dependent inertia matrix. In fact, as is evident in Figs. 5a and 5b, the comparison controller shows significantly diminished asymptotic convergence compared to the proposed controller. For smaller times, the comparison controller shows reduction in error norms, however, the error norms saturate around 0.5 deg/s for angular velocity and near 0.001 for the quaternion error. In contrast, the proposed controller drives the

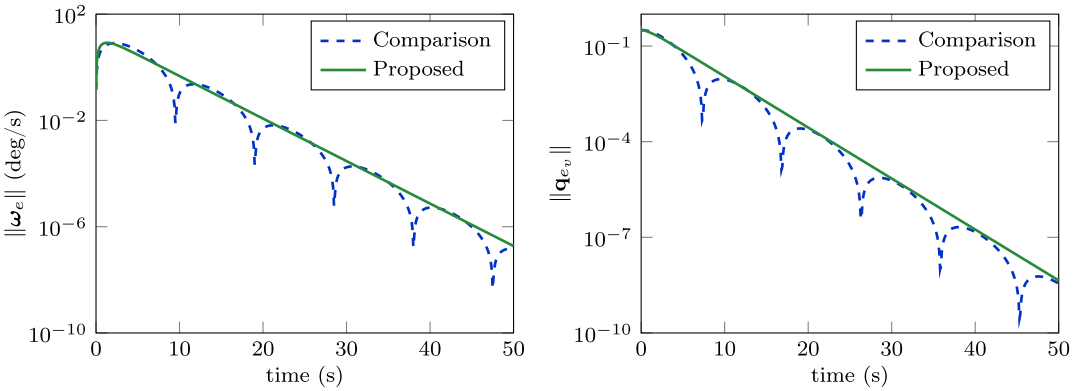

a) Norm of angular velocity error vector **b) Norm of quaternion error vector**

Fig. 3 Baseline performance of proposed and comparison controllers, generated using constant and known J_0 in Eq. (61).

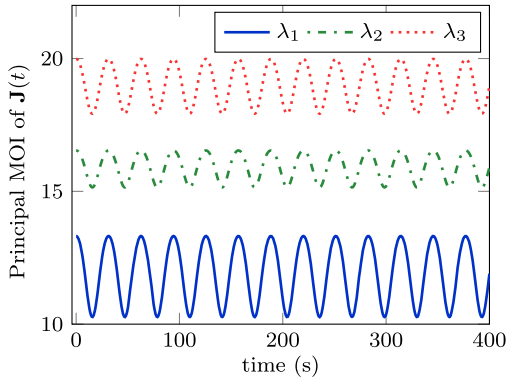

Fig. 4 Principal moments of inertia (MOI) of time-dependent $J(t)$ for a spacecraft with moving parts.

angular velocity tracking error norm to below 0.001 deg /s and the quaternion error vector norm to below 1×10^{-4} within 400 s.

The degradation of performance in the comparison control is considered to be a direct result of significant inertia matrix changes, which are not explicitly taken into account as they are in the proposed control law. Thus, at best, the comparison controller is only able to drive the tracking errors to within a bounded set. In Fig. 5d, observe that the proposed controller has a slightly higher overshoot in the initial transient regime. However, the steady-state regime in Fig. 5c seems to indicate that the comparison controller actually commands a higher overall control torque norm than the proposed controller. The higher control demand stems from the fact that, because the comparison controller does not directly take into account the time-varying inertia components, it expends a significant amount of effort adapting to parameters that are rapidly varying. Note that the steady-state control is time varying because a time-varying trajectory is being tracked. Finally, it is noted that, because the underlying reference trajectory does not satisfy PE conditions, the parameter estimates are not expected to converge to their true values. This is clearly the case for $\hat{\boldsymbol{\theta}}$ in Fig. 6a. However, as illustrated in Fig. 6b, the added excitation due to the sinusoidal variation in Ψ allows J_1 estimates $\hat{\boldsymbol{\sigma}}$ to converge to their true values.

B. Fuel Loss Compensation

Next, numerical simulations are conducted for a spacecraft undergoing inertia matrix changes due to fuel mass loss. In particular, the inertia matrix variations are described by Eq. (17), the adaptive control is given by Eqs. (37) and (44), and the parameter estimation update laws with smooth projection in Eqs. (30) and (34) are simulated. Using $\boldsymbol{\rho} = 0$ in Eq. (17), the unknown matrix J_1 is taken as the diagonal matrix

$$J_1 = \begin{bmatrix} 4 \times 10^{-3} & 0 & 0 \\ 0 & 4 \times 10^{-3} & 0 \\ 0 & 0 & 5 \times 10^{-3} \end{bmatrix}$$

which essentially models a fuel tank in the shape of a cylinder whose center of mass is collocated with the center of mass of the overall spacecraft. Consistent with the remarks made following Theorem 3, the constant $\lambda_{\max}$ is taken to be the maximum eigenvalue of J_0, that is, $\lambda_{\max} = 20.7352$, whereas the minimum eigenvalue is taken as $\lambda_{\min} = 0.5$ and is assumed to be the eigenvalue associated with the dry mass inertia matrix of the spacecraft.

The constants for convex sets Ω_{θ^*} and $\Omega_{\hat{\theta}}$ are $\epsilon_1 = (40)^2$ and $\delta_1 = (10)^2$, and those for Ω_{σ^*} and $\Omega_{\hat{\sigma}}$ are given by $\epsilon_2 = (0.008)^2$ and $\delta_2 = (0.008)^2$. Note that $\|\boldsymbol{\theta}^*\|^2 \in \Omega_{\theta^*}$, $\|\boldsymbol{\sigma}^*\|^2 \in \Omega_{\sigma^*}$, and the initial conditions $\hat{\boldsymbol{\theta}}(0) = [21.1, 1.9, 1.4, 17.8, 2.9, 15.5]^T$ and $\hat{\boldsymbol{\sigma}}(0) = 0$ belong, respectively, to sets $\Omega_{\hat{\theta}}$ and $\Omega_{\hat{\sigma}}$. Furthermore, $\omega_B = \sup_{t \geq 0} \|\boldsymbol{\omega}_r\| = 1.1832$ and $\zeta^* = 55.56$. The tuning parameters are selected to be

$$\gamma = 100, \qquad \gamma_1 = 8, \qquad \gamma_2 = 20.5$$

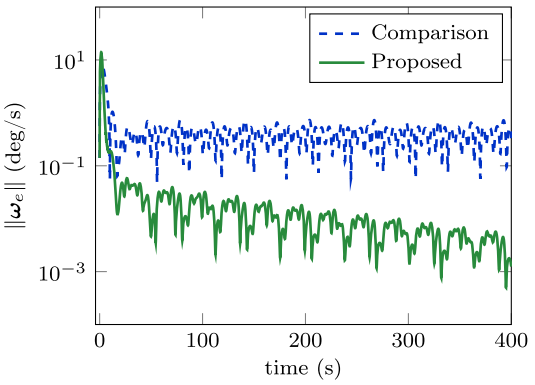

a) Norm of angular velocity error vector

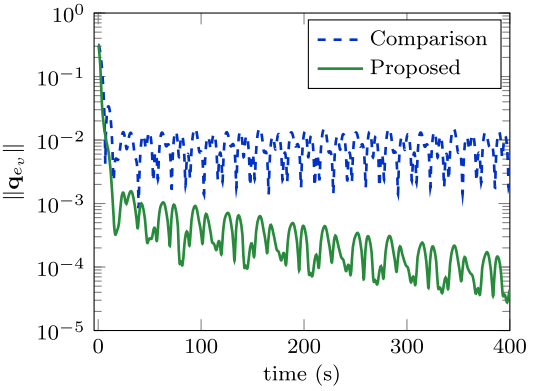

b) Norm of quaternion error vector

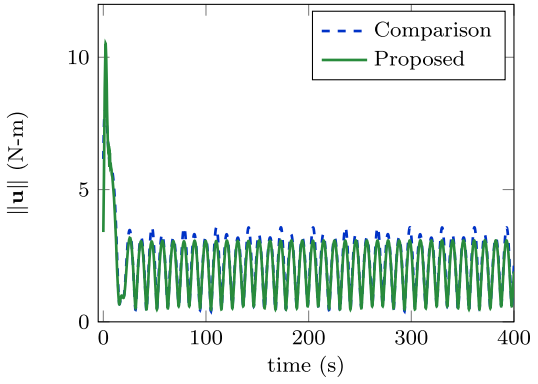

c) Norm of control vector

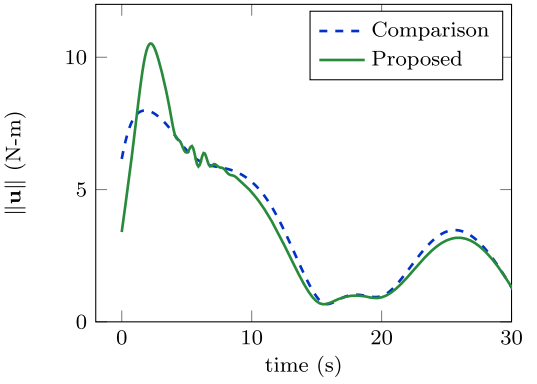

d) Initial transient of control norm

Fig. 5 Adaptive attitude-tracking control simulation for spacecraft with time-dependent inertia matrix variations due to mass displacement.

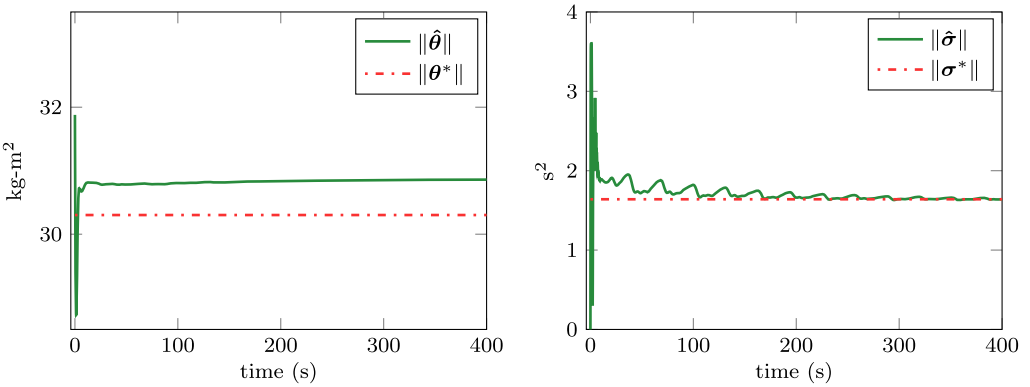

a) Norm of $\mathbf{J_0}$ parameter estimates, $\|\hat{\boldsymbol{\theta}}\|$ **b) Norm of $\mathbf{J_1}$ parameter estimates, $\|\hat{\boldsymbol{\sigma}}\|$**

Fig. 6 Parameter estimates of the unknown J_0 and J_1 matrices for mass-displacement example.

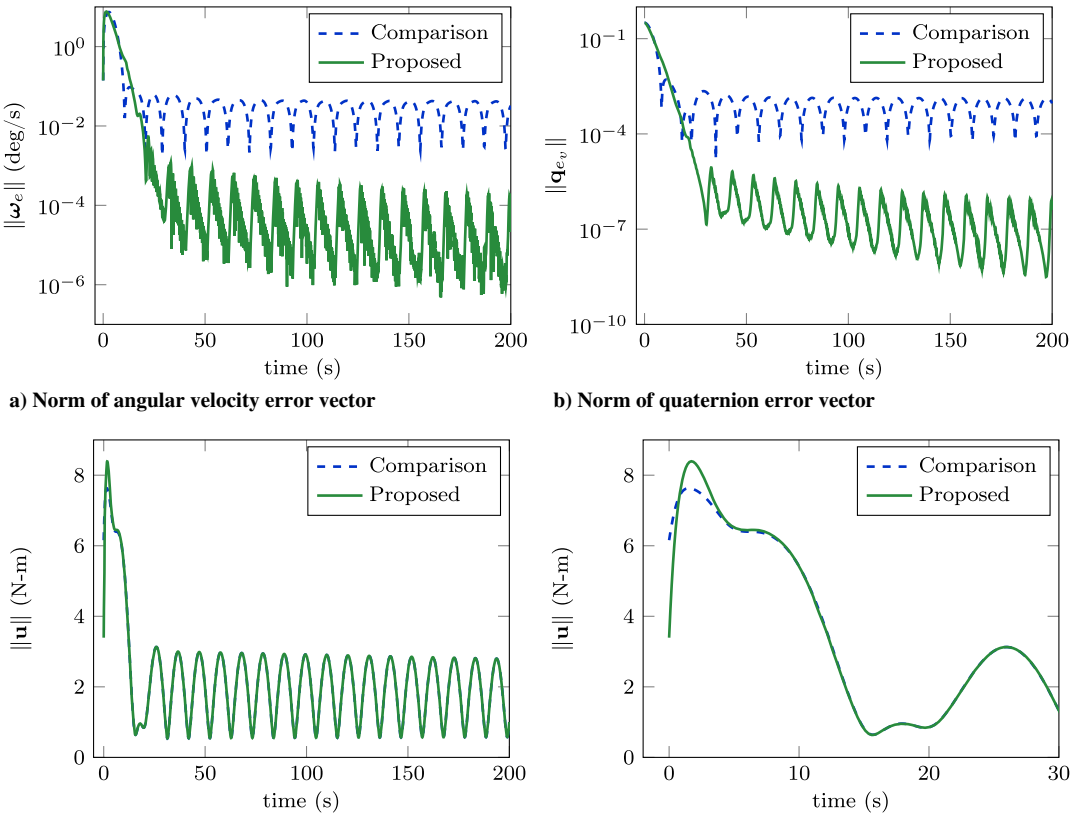

a) Norm of angular velocity error vector **b) Norm of quaternion error vector**

c) Norm of control vector **d) Initial transient of control norm**

Fig. 7 Adaptive attitude-tracking control response for a spacecraft with fuel mass-loss-induced inertia variations.

and are chosen in such a manner to yield a result closest to the baseline performance for each controller. Moreover, using the selected parameters, the following inequality is obtained in accordance with Eq. (50):

$$(\|\boldsymbol{\omega}_e(0)\|+1)^2 < \frac{2}{\lambda_{\max}}\left[\frac{\lambda_{\min}}{2}(\zeta^*-1)^2 - \frac{\lambda_{\min}}{2} - 4(\beta+k_v) - \frac{(\sqrt{\epsilon_1+\delta_1}+\sqrt{\epsilon_1})^2}{2\gamma_1} - \frac{(\sqrt{\epsilon_2+\delta_2}+\sqrt{\epsilon_2})^2}{2\gamma_2}\right] \approx 14.81$$

which is readily satisfied for $\|\boldsymbol{\omega}_e(0)\| = 0.0024$, thereby ensuring a nonsingular control for the entire duration of the simulation. Note that every effort was made by the authors to select the best possible tuning parameters for each control method. The results are illustrated in Figs. 7 and 8.

As with the appendage deployment case, it is found that, although the proposed controller is able to drive the attitude and angular velocity errors to the origin in a consistent manner, the comparison controller suffers from an appreciable loss of accuracy both for attitude and angular velocity tracking. The norms of the control torques commanded by the proposed and comparison controllers are shown in Figs. 7c and 7d. The proposed control law remains well defined throughout the simulation period. As illustrated in Fig. 7d, the torque demands of both controllers are comparable during the initial transient period. In Fig. 7c, the monotonic steady-state decay of the control norm for both controllers is consistent with the decrease in the overall rotational inertia of the spacecraft as a consequence of losing mass.

The time evolution of the parameter estimates is shown in Fig. 8. In Fig. 8b, a similar trend to the deployment scenario is found, where the update law for $\hat{\boldsymbol{\sigma}}$ in the proposed control strategy is able to drive the estimated values to their true values. As mentioned in the preceding

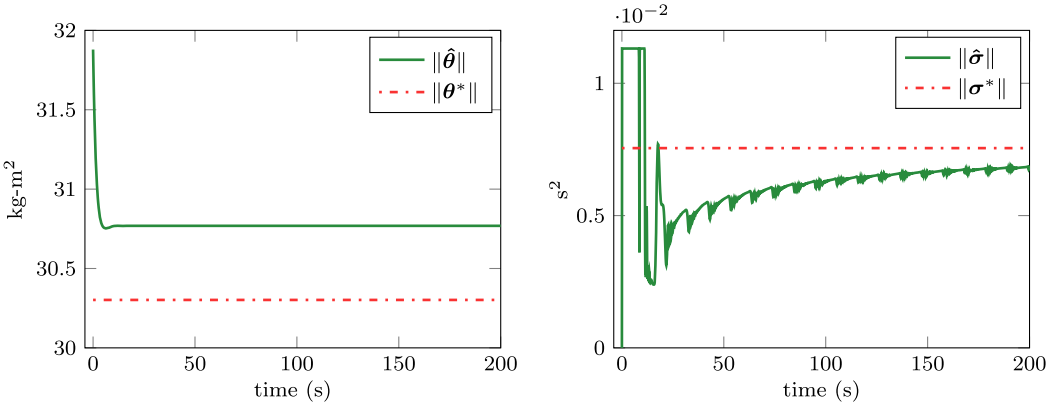

a) Norm of $\mathbf{J}_0$ parameter estimates, $\|\hat{\boldsymbol{\theta}}\|$ **b) Norm of $\mathbf{J}_1$ parameter estimates, $\|\hat{\boldsymbol{\sigma}}\|$**

Fig. 8 Parameter estimates of unknown J_0 and J_1 matrices (fuel loss example).

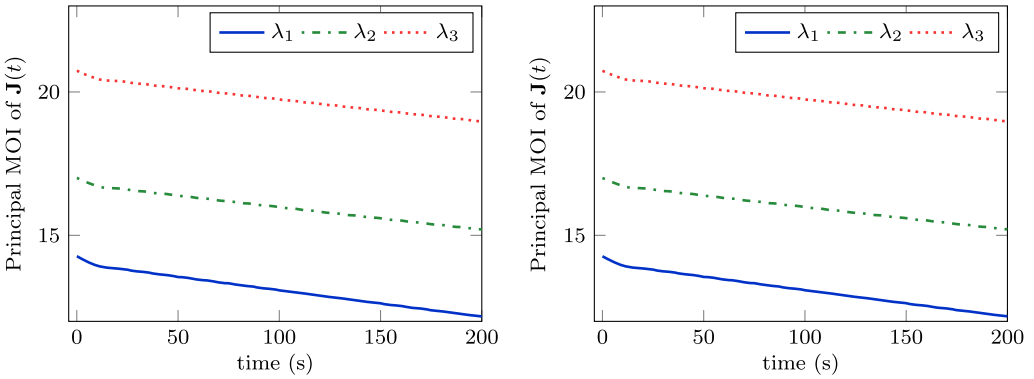

a) Proposed controller **b) Comparison controller**

Fig. 9 Principal moments of inertia of the control-norm-dependent inertia matrix simulating variations due to fuel mass loss.

example, the added persistence of excitation introduced in W_2 and W_3, due to the input-dependent Ψ and $\dot{\Psi}$ matrices, contributes to this unique feature despite a non-PE reference trajectory. Furthermore, as expected, $\|\hat{\boldsymbol{\sigma}}\|$ is bounded by $\sqrt{\epsilon_2 + \delta_2} = 0.0113$ due to the smooth projection mechanism. Finally, the evolution of the principal moments of inertia of the fuel-mass-dependent inertia matrix is illustrated in Fig. 9a for the proposed controller and in Fig. 9b for the comparison controller. The simulated inertia matrix remains positive definite and satisfies the triangle inequalities in Eq. (9) for all time.

VI. Conclusions

In this investigation, an adaptive attitude control problem is addressed for a spacecraft with a time-varying inertia matrix. The inertia matrix consists of an unknown rigid (constant) matrix component, as well as a partially known variable component with multiplicative uncertainty. The variable inertia term may be purely input dependent or may display a combination of time and/or state dependencies. The proposed adaptive control delivers consistent tracking performance in the face of arbitrarily large uncertainties in the inertia matrix. When variations occur due to fuel mass loss, a smooth projection scheme prevents drifting of the parameter estimates and ensures a singularity-free control solution for the coupled dynamics, resulting from a control torque-dependent inertia matrix. A complete analysis of the proposed control law depicting asymptotic convergence of the tracking error signals is provided. Numerical simulation examples are provided to highlight the performance gains of the proposed controller when compared to an existing adaptive controller that does not account for inertia variations. The proposed control scheme has many practical advantages, especially in the field of aerospace engineering, where spacecraft often experience mass displacement or variations during flight.

References

[1] Wen, J. T., and Kreutz-Delgado, K., "Attitude Control Problem," *IEEE Transactions on Automatic Control*, Vol. 36, No. 10, 1991, pp. 1148–1162. doi:10.1109/9.90228

[2] Costic, B. T., Dawson, D. M., de Queiroz, M. S., and Kapila, V., "Quaternion-Based Adaptive Attitude Tracking Controller Without Velocity Measurements," *Journal of Guidance, Control, and Dynamics*, Vol. 24, No. 6, 2001, pp. 1214–1222. doi:10.2514/2.4837

[3] Seo, D., and Akella, M. R., "High-Performance Spacecraft Adaptive Attitude-Tracking Control Through Attracting-Manifold Design," *Journal of Guidance, Control, and Dynamics*, Vol. 31, No. 4, 2008, pp. 884–891. doi:10.2514/1.33308

[4] Ahmed, J., and Bernstein, D. S., "Globally Convergent Adaptive Control of Spacecraft Angular Velocity Without Inertia Modeling," *Proceedings of the American Control Conference*, Vol. 3, No. 1, 1999, pp. 1540–1544. doi:10.1109/ACC.1999.786083

[5] Astolfi, A., and Ortega, R., "Immersion and Invariance: A New Tool for Stabilization and Adaptive Control of Nonlinear Systems," *IEEE Transactions on Automatic Control*, Vol. 48, No. 4, 2003, pp. 590–606. doi:10.1109/TAC.2003.809820

[6] Kárason, S. P., and Annaswamy, A. M., "Adaptive Control in the Presence of Input Constraints," *IEEE Transactions on Automatic Control*, Vol. 39, No. 11, 1994, pp. 2325–2330. doi:10.1109/9.333787

[7] Annaswamy, A. M., and Narendra, K. S., "Adaptive Control of Simple Time Varying Systems," *Proceedings of the 28th IEEE Conference on Decision and Control*, Vol. 2, IEEE Publications, Piscataway, NJ, 1989, pp. 1014–1018.

[8] Middleton, R. H., and Goodwin, G. C., "Adaptive Control of Time-Varying Linear Systems," *IEEE Transactions on Automatic Control*, Vol. 33, No. 2, 1988, pp. 150–155. doi:10.1109/9.382

[9] Zhang, Y., and Ioannou, P., "Adaptive Control of Linear Time Varying Systems," *Proceedings of the 35th IEEE Conference on Decision and Control*, IEEE Publications, Piscataway, NJ, 1996, pp. 837–842.

[10] Ioannou, P. A., and Sun, J., *Robust Adaptive Control*, Dover, New York, 2012, pp. 634–768.
[11] Xu, J., "New Periodic Adaptive Control Approach for Time-Varying Parameters with Known Periodicity," *IEEE Transactions on Automatic Control*, Vol. 48, No. 8, 2003, pp. 579–583.
[12] Ge, S. S., and Wang, J., "Robust Adaptive Tracking for Time-Varying Uncertain Nonlinear Systems with Unknown Control Coefficients," *IEEE Transactions on Automatic Control*, Vol. 48, No. 8, 2003, pp. 1463–1469. doi:10.1109/TAC.2003.815049
[13] Yucelen, T., and Haddad, W. M., "Low-Frequency Learning and Fast Adaptation in Model Reference Adaptive Control," *IEEE Transactions on Automatic Control*, Vol. 58, No. 4, 2013, pp. 1080–1085. doi:10.1109/TAC.2012.2218667
[14] Yucelen, T., "Adaptive Spacecraft Control: Stability, Performance, and Robustness," *Proceedings of the AIAA Guidance, Navigation, and Control Conference*, AIAA, Reston, VA, 2013. doi:10.2514/6.2013-4934
[15] Weiss, A., Kolmanovsky, I., and Bernstein, D., "Inertia-Free Attitude Control of Spacecraft with Unknown Time-Varying Mass Distribution," *62nd International Astronautical Congress*, Paper IAC-11-C1.5.9, 2011.
[16] Sastry, S., and Bodson, M., *Adaptive Control: Stability, Convergence, and Robustness*, Prentice–Hall, Upper Saddle River, NJ, 1989, pp. 99–157, Chap. 3.
[17] Schaub, H., and Junkins, J., *Analytical Mechanics of Space Systems*, AIAA Education Series, AIAA, Reston, VA, 2003, pp. 63–114, Chap. 3.
[18] Shuster, M. D., "Survey of Attitude Representation," *Journal of Astronautical Sciences*, Vol. 41, No. 4, 1993, pp. 439–517.
[19] Wie, B., *Space Vehicle Dynamics and Control*, AIAA Education Series, AIAA, Reston, VA, 1998, pp. 381–460, Chap. 7.
[20] Khalil, H. K., "Adaptive Output Feedback Control of Nonlinear Systems Represented by Input-Output Models," *IEEE Transactions on Automatic Control*, Vol. 41, No. 2, 1996, pp. 177–188. doi:10.1109/9.481517
[21] Yoon, H., and Tsiotras, P., "Adaptive Spacecraft Attitude Tracking Control with Actuator Uncertainties," *Journal of Astronautical Sciences*, Vol. 56, No. 2, 2008, pp. 251–268. doi:10.1007/BF03256551